

Supporting Information:

Cation disorder dominates the defect chemistry of high-voltage $\text{LiMn}_{1.5}\text{Ni}_{0.5}\text{O}_4$ (LMNO) spinel cathodes

Jiayi Cen,^{†,‡} Bonan Zhu,^{†,‡} Seán R. Kavanagh,^{†,¶} Alexander G. Squires,^{†,‡} and
David O. Scanlon^{*,†,‡}

[†]*Department of Chemistry and Thomas Young Centre, University College London, 20
Gordon Street, London WC1H 0AJ, United Kingdom*

[‡]*The Faraday Institution, Quad One, Harwell Science and Innovation Campus, Didcot
OX11 0RA, United Kingdom*

[¶]*Department of Materials and Thomas Young Centre, Imperial College London, Exhibition
Road, London SW7 2AZ, United Kingdom*

E-mail: d.scanlon@ucl.ac.uk

Supporting Information Available

Implications of DFT + U vs hybrid DFT

The localised d electrons in open-shell transition metals (TM) oxides give rise to strong on-site Coulomb interaction that standard density functional theory (DFT) methods approximate poorly, giving incorrect electronic structures. DFT + U and hybrid functional

calculations are two popular methods to improve the description of the localised electrons, giving closer approximations to the true geometry and electronic structure. The hybrid approach incorporates exact exchange from Hartree-Fock yielding methods such as PBE0 and HSE.^{S1,S2} This method is computationally demanding and is only practically feasible with small-medium sized systems (< 200 atoms). The DFT + U approach applies empirical on-site correction, thus alleviating the problem at a much lower computational cost, but this method is subject to a few limitations. In theory, U parameter is sensitive to chemical environments, meaning that different U values would be needed for the same species depending on their environments. A universal U would give incorrect relative energies between systems with a mixture of localised and delocalised states.^{S3} For example, applying the same U value on the atomic sites in metallic states and in the metal oxides. Using a single U per species across compounds with similar chemical environments, however, can give accurate energies due to error cancellations.^{S4} Santana *et al.*^{S3} performed GGA + U calculations with a range of U values ($U = 1.5, 3.3, 5.0$ and 5.5 eV) on competing phases of LiCoO_2 as part of the defect study and found the chemical potential ranges to be dependent on the U values.

We acknowledge that hybrid functional calculations are generally more reliable than the DFT + U approach and hence have compared the electronic structure computed using the PBEsol + U with HSE06. The large supercell size (448-atom) poses exorbitant computational cost for defect calculations, thus we use PBEsol + U to calculate all the defect properties. Nevertheless, DFT + U was proven to be an effective approach to model the polaronic behaviours in correlated materials with improved description of localised states and the band gap.^{S5} We expect the PBEsol + U results to be qualitatively similar to HSE06. Given that LMNO is a weak semiconductor, band shifting (due to different predicted band gaps) would not change the results significantly.

Dielectric constant calculations

The static dielectric constant (ϵ_0) was 11.73, with contributions from high-frequency electronic/optical (ϵ_{optic}) of 6.36 and low-frequency lattice/ionic (ϵ_{ionic}) of 5.37, with convergence checking.

Table S1: ϵ_{ionic} convergence data with respect to energy cutoff (ENCUT), calculated using **k**-point $3 \times 3 \times 3$. ϵ_{ionic} is converged at 450 eV. ϵ_{ionic} in the x , y and z directions are the same by symmetry.

ENCUT [eV]	ϵ_{ionic}	$\Delta \epsilon_{\text{ionic}}$
350	5.24	0.15
400	5.26	0.13
450	5.37	0.02
500	5.39	0.01
550	5.37	0.02
600	5.37	0.03
650	5.36	0.03
700	5.36	0.03
750	5.39	0.00
800	5.39	0.00

Table S2: ϵ_{ionic} convergence data with respect to **k**-point, calculated using 550 eV energy cutoff. ϵ_{ionic} is converged at **k**-point $3 \times 3 \times 3$. ϵ_{ionic} in the x , y and z directions are the same by symmetry.

KPOINTS	ϵ_{ionic}	$\Delta \epsilon_{\text{ionic}}$
$2 \times 2 \times 2$	5.36	0.01
$3 \times 3 \times 3$	5.37	0.00
$4 \times 4 \times 4$	5.37	0.00
$5 \times 5 \times 5$	5.37	0.00
$6 \times 6 \times 6$	5.37	0.00
$7 \times 7 \times 7$	5.37	0.00

Table S3: ϵ_{optic} convergence data with respect to NBANDS, calculated with 550 eV energy cutoff and \mathbf{k} -point $3 \times 3 \times 3$. ϵ_{optic} is converged at NBANDS = 420. ϵ_{optic} in the x , y and z directions are the same by symmetry.

NBANDS	ϵ_{optic}	$\Delta \epsilon_{\text{optic}}$
240	3.04	3.41
260	5.18	1.27
280	5.64	0.81
300	5.88	0.57
320	6.09	0.36
340	6.03	0.42
360	6.20	0.25
380	6.17	0.29
400	6.29	0.16
420	6.36	0.09
440	6.38	0.07
460	6.38	0.08
480	6.28	0.18
500	6.37	0.08
520	6.45	0.00

The magnetic ordering of bulk LMNO

The $P4_332$ LMNO has Mn^{4+} (d^3) and Ni^{2+} (d^2) in the octahedral (O_h) sites, thus both populating the t_{2g} orbitals according to Hund’s rule, giving magnetic moments of $3 \mu_B$ and $2 \mu_B$ for Mn and Ni respectively. The magnetic enumeration generated 47 unique combinations in their ferromagnetic (FM), ferrimagnetic (FiM) and antiferromagnetic (AFM) states. A spread of DFT energies is observed for the different spin initialisations (Figure S1). There is a linear relationship between the energies before and after geometry relaxation, suggesting that one could potentially use single point calculations to screen out the unfavourable spin configurations, provided that “spin-flip” does not occur during relaxations. The data point with the lowest energy before and after relaxation has the FiM arrangement, where $\text{Mn}\uparrow \text{Ni}\downarrow$. An experimental magnetisation study^{S6} found a net magnetisation of $3.1 \mu_B$ per formula unit, which is close to the calculated value of $3.5 \mu_B$. The deviation between the values can be attributed to imperfection in the sample, for instance, a small proportion of inverse spinel due to Mn populating the tetrahedral (T_d) sites.

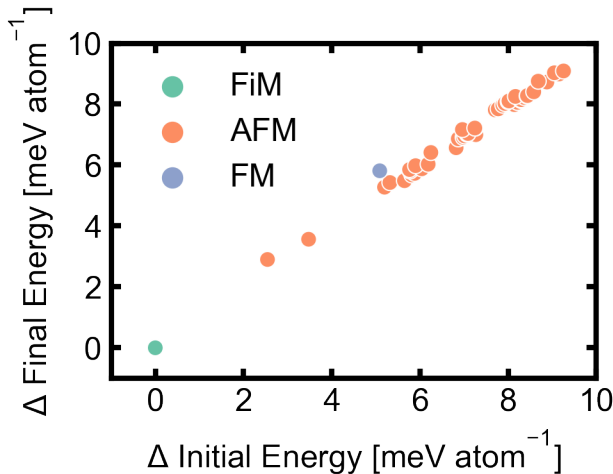


Figure S1: A scatter plot of the DFT energy difference per atom relative to the lowest energy value before and after geometry relaxation. Each point corresponds to a distinct magnetic ordering initialisation, and is classified into ferromagnetic (FM), ferrimagnetic (FiM) and antiferromagnetic (AFM) ordering. The data point with lowest initial and final energy corresponds to the ferrimagnetic arrangement with $\text{Mn}\uparrow \text{Ni}\downarrow$.

The anti-parallel spin (i.e. AFM interaction) between Mn and Ni arises from the oxygen-

mediated super-exchange where the spin information is transferred through covalent interactions with the intervening oxygen ligands. Since the cubic geometry leads to a number of competitive metal-metal interactions, the interaction with the greatest orbital overlap integral would dominate.^{S7,S8} In this case, the AFM $\text{Ni}^{2+}:e_g^2$ -O: $2p_{\pi\sigma}$ - $\text{Mn}^{4+}:t_{2g}^3$ dominates over other FM interactions. The energy difference between the most stable and least stable magnetic orderings was calculated to be 9.15 meV atom⁻¹, with the FM ordering lying 5.81 meV atom⁻¹ above the FiM ground state, in line with experimental findings.^{S6}

Electronic band structure

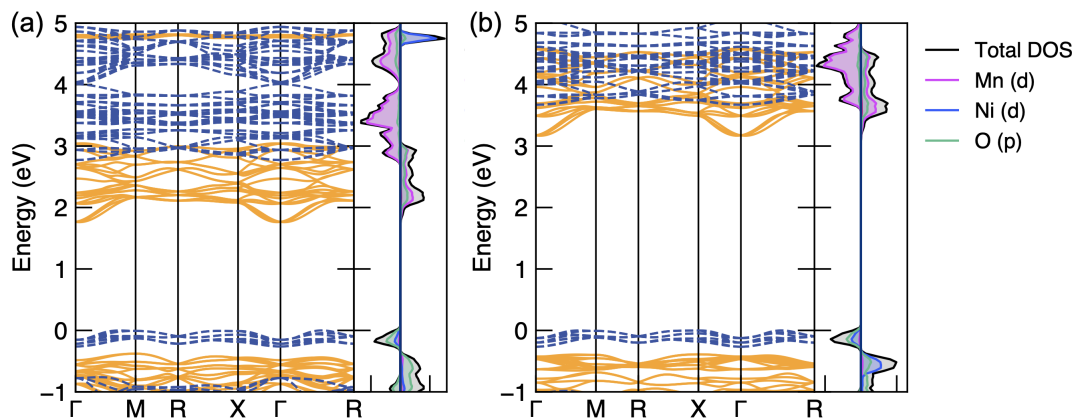


Figure S2: The electronic band structures and density of states of $P4_332$ $\text{LiMn}_{1.5}\text{Ni}_{0.5}\text{O}_4$ obtained from (a) PBEsol + U and (b) HSE06 calculations. The valence band maximum was set to 0 eV. The blue dashed and solid orange lines correspond to the spin-down and spin-up channel, respectively.

Stable phases

Table S4: Constituent elemental phases of $\text{LiMn}_{1.5}\text{Ni}_{0.5}\text{O}_4$ calculated using the specified \mathbf{k} -points in their standard states. Formation energies of elemental phases are zero by definition.

Species	Space Group	\mathbf{k} -point
Li	$R\bar{3}m$	$17 \times 17 \times 17$
Mn	$I\bar{4}3m$	$6 \times 6 \times 6$
Ni	$Fm\bar{3}m$	$21 \times 21 \times 21$
O	$P\bar{1}$	$1 \times 1 \times 1$

Table S5: Formation energies of stable competing phases of $\text{LiMn}_{1.5}\text{Ni}_{0.5}\text{O}_4$ ($\text{Li}_2\text{Mn}_3\text{NiO}_8$) calculated with specified \mathbf{k} -points.

System	Space group	\mathbf{k} -point	Formation energy [eV atom ⁻¹]
$\text{Li}_2\text{Mn}_3\text{NiO}_8$	$P4_332$	$3 \times 3 \times 3$	-2.40
$\text{Li}_5\text{Mn}_7\text{O}_{16}$	$Pnmm$	$5 \times 3 \times 3$	-2.50
$\text{Li}_4\text{Mn}_5\text{O}_{12}$	$C2/c$	$5 \times 5 \times 2$	-2.45
Mn_5O_8	$C2/m$	$5 \times 5 \times 5$	-2.74
$\text{Mn}(\text{Ni}_3\text{O}_4)_2$	$P1$	$5 \times 5 \times 5$	-1.89
LiMn_2O_4	$Pnma$	$3 \times 3 \times 3$	-2.59
Mn_2O_3	$Pbca$	$3 \times 3 \times 3$	-2.82
$\text{Li}_2\text{Ni}_2\text{O}_3$	$P\bar{1}$	$8 \times 5 \times 3$	-1.81
MnNiO_3	$R\bar{3}$	$6 \times 6 \times 6$	-2.22
Li_2NiO_3	$C2/m$	$7 \times 7 \times 7$	-1.64
LiMnO_2	$C2/m$	$5 \times 9 \times 5$	-2.61
Mn_3O_4	$I4_1/amd$	$4 \times 4 \times 3$	-2.95
Li_2NiO_2	$P\bar{3}m1$	$8 \times 8 \times 5$	-1.84
MnO_2	Pm	$3 \times 3 \times 8$	-2.42
LiNiO_2	$P2_1/c$	$5 \times 9 \times 6$	-1.68
Li_2O_2	$P6_3/mmc$	$9 \times 9 \times 4$	-1.49
MnO	$I4/mmm$	$6 \times 6 \times 6$	-3.11
Li_2O	$Fm\bar{3}m$	$9 \times 9 \times 9$	-1.89
NiO	$I4/mmm$	$6 \times 6 \times 6$	-1.71
Li_2MnO_3	$C2/m$	$6 \times 6 \times 6$	-2.42
Li_6MnO_4	$P4_2/nmc$	$4 \times 4 \times 5$	-2.11
MnNi	$Pm\bar{3}m$	$13 \times 13 \times 13$	-1.45
MnNi_3	$Pm\bar{3}m$	$12 \times 12 \times 12$	-0.76

Chemical Potential Limits

Table S6: Intersection points of atomic chemical potentials bounding the stability region of the host ($\text{Li}_2\text{Mn}_3\text{NiO}_8$) from CPLAP, where μ_{O} was set as the dependent variable.

Facet Name	Label	μ_{Li} [eV]	μ_{Mn} [eV]	μ_{Ni} [eV]	μ_{O} [eV]
$\text{Li}_2\text{Mn}_3\text{NiO}_8\text{-Li}_2\text{MnO}_3\text{-NiO-O}_2$	A	-3.35	-7.81	-3.42	0.00
$\text{Li}_4\text{Mn}_5\text{O}_{12}\text{-Li}_2\text{Mn}_3\text{NiO}_8\text{-Li}_2\text{MnO}_3\text{-O}_2$	B	-3.51	-7.50	-4.05	0.00
$\text{Mn}(\text{Ni}_3\text{O}_4)_2\text{-Li}_2\text{Mn}_3\text{NiO}_8\text{-NiO-O}_2$	C	-3.45	-7.75	-3.42	0.00
$\text{Mn}(\text{Ni}_3\text{O}_4)_2\text{-Li}_2\text{Mn}_3\text{NiO}_8\text{-MnNiO}_3\text{-O}_2$	D	-3.58	-7.65	-3.44	0.00
$\text{Li}_4\text{Mn}_5\text{O}_{12}\text{-Li}_2\text{Mn}_3\text{NiO}_8\text{-Li}_5\text{Mn}_7\text{O}_{16}\text{-O}_2$	E	-3.74	-7.32	-4.14	0.00
$\text{Li}_4\text{Mn}_5\text{O}_{12}\text{-Li}_2\text{Mn}_3\text{NiO}_8\text{-Li}_5\text{Mn}_7\text{O}_{16}\text{-Li}_2\text{MnO}_3$	F	-3.37	-6.95	-3.78	-0.27
$\text{MnO}_2\text{-Li}_2\text{Mn}_3\text{NiO}_8\text{-Li}_5\text{Mn}_7\text{O}_{16}\text{-O}_2$	G	-3.81	-7.26	-4.15	0.00
$\text{MnO}_2\text{-Li}_2\text{Mn}_3\text{NiO}_8\text{-MnNiO}_3\text{-O}_2$	H	-3.97	-7.26	-3.83	0.00
$\text{MnO}_2\text{-Li}_2\text{Mn}_3\text{NiO}_8\text{-MnNiO}_3\text{-Mn}_5\text{O}_8$	I	-3.81	-6.59	-3.50	-0.33
$\text{MnO}_2\text{-Li}_2\text{Mn}_3\text{NiO}_8\text{-Li}_5\text{Mn}_7\text{O}_{16}\text{-Mn}_5\text{O}_8$	J	-3.68	-6.59	-3.75	-0.33
$\text{LiMn}_2\text{O}_4\text{-Li}_2\text{Mn}_3\text{NiO}_8\text{-Li}_5\text{Mn}_7\text{O}_{16}\text{-Mn}_5\text{O}_8$	K	-3.41	-6.14	-3.38	-0.62
$\text{LiMn}_2\text{O}_4\text{-Li}_2\text{Mn}_3\text{NiO}_8\text{-Li}_5\text{Mn}_7\text{O}_{16}\text{-Li}_2\text{MnO}_3$	L	-3.02	-5.75	-3.00	-0.91
$\text{LiMn}_2\text{O}_4\text{-Mn}_2\text{O}_3\text{-Li}_2\text{Mn}_3\text{NiO}_8\text{-Mn}_5\text{O}_8$	M	-3.39	-6.10	-3.35	-0.64
$\text{Mn}_2\text{O}_3\text{-Li}_2\text{Mn}_3\text{NiO}_8\text{-MnNiO}_3\text{-Mn}_5\text{O}_8$	N	-3.53	-6.10	-3.07	-0.64
$\text{LiMn}_2\text{O}_4\text{-Mn}_2\text{O}_3\text{-Li}_2\text{Mn}_3\text{NiO}_8\text{-Mn}_3\text{O}_4$	O	-2.93	-5.41	-2.66	-1.10
$\text{LiMn}_2\text{O}_4\text{-Li}_2\text{Mn}_3\text{NiO}_8\text{-Mn}_3\text{O}_4\text{-Li}_2\text{MnO}_3$	P	-2.85	-5.34	-2.59	-1.16
$\text{Li}_2\text{Mn}_3\text{NiO}_8\text{-Mn}_3\text{O}_4\text{-Li}_2\text{MnO}_3\text{-NiO}$	Q	-2.66	-5.02	-2.03	-1.40
$\text{Mn}(\text{Ni}_3\text{O}_4)_2\text{-Li}_2\text{Mn}_3\text{NiO}_8\text{-Mn}_3\text{O}_4\text{-NiO}$	R	-2.80	-5.14	-2.12	-1.30
$\text{Mn}_2\text{O}_3\text{-Li}_2\text{Mn}_3\text{NiO}_8\text{-Mn}_3\text{O}_4\text{-MnNiO}_3$	S	-3.07	-5.41	-2.38	-1.10
$\text{Mn}(\text{Ni}_3\text{O}_4)_2\text{-Li}_2\text{Mn}_3\text{NiO}_8\text{-Mn}_3\text{O}_4\text{-MnNiO}_3$	T	-3.00	-5.33	-2.27	-1.16

Initial Interstitial Positions

Table S7: The Wyckoff positions for the unrelaxed (standard) interstitial sites in the supercell and their corresponding positions in the primitive cell.

Position	Supercell	Primitive cell
1	192 <i>e</i>	24 <i>e</i>
2	192 <i>e</i>	24 <i>e</i>
3	192 <i>e</i>	24 <i>e</i>
4	192 <i>e</i>	24 <i>e</i>
5	96 <i>d</i>	12 <i>d</i>
6	96 <i>d</i>	12 <i>d</i>

Octahedral volumes

Table S8: Calculated volume of octahera at the 4*a* and 12*d* sites.

Sites	Volume [\AA^3]
4 <i>a</i>	12.51
12 <i>d</i>	11.79

Relaxed configurations of lithium interstitials

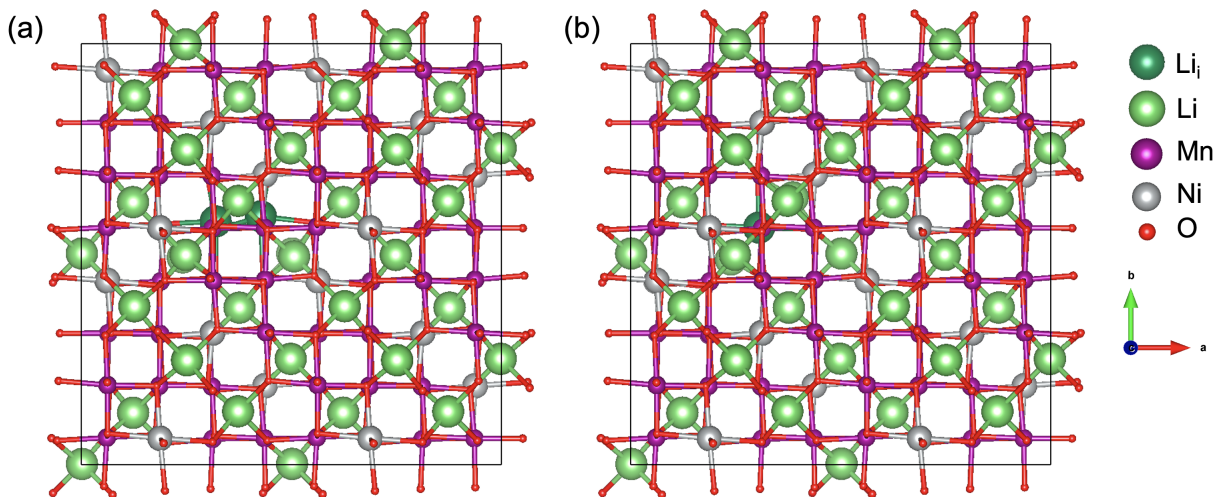


Figure S3: The relaxed configurations of lithium interstitials existing as a Li-Li dumbbell configuration (a) and in a conventional interstitial site (b).

Relaxed configurations of peroxides

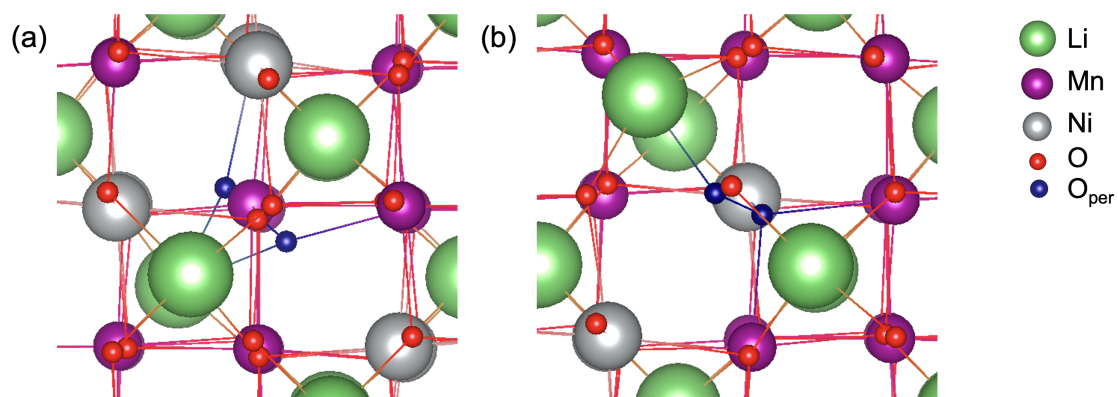


Figure S4: The relaxed configurations of peroxides where the centre of mass of the O-dumbbell resides on (a) a defined lattice site (lower in energy) (b) a distorted site (higher in energy) unfavourably displacing neighbouring Li⁺ away from its 8c crystal sites.

Concentration of oxygen vacancies

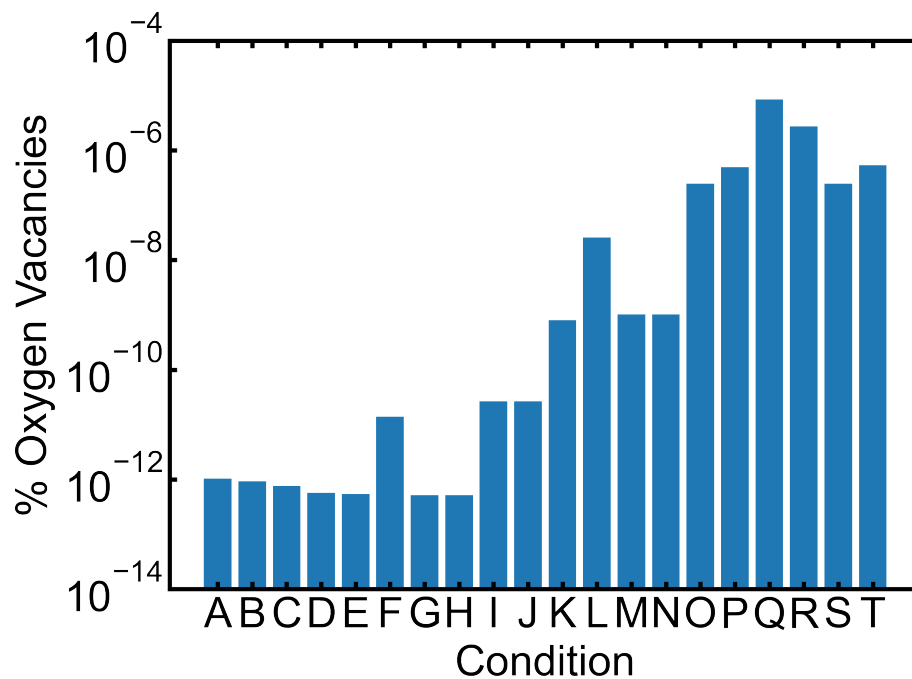


Figure S5: The total concentration of oxygen vacancies (expressed as site percentages) over all growth conditions, calculated at the self-consistent Fermi level with temperature set to 973 K.

References

- (S1) Heyd, J.; Scuseria, G. E.; Ernzerhof, M. Hybrid Functionals Based on a Screened Coulomb Potential. *J. Chem. Phys.* **2003**, *118*, 8207–8215.
- (S2) Adamo, C.; Barone, V. Toward Reliable Density Functional Methods without Adjustable Parameters: The PBE0 Model. *J. Chem. Phys.* **1999**, *110*, 6158–6170.
- (S3) Santana, J. A.; Kim, J.; Kent, P. R. C.; Reboredo, F. A. Successes and Failures of Hubbard-corrected Density Functional Theory: The Case of Mg Doped LiCoO₂. *J. Chem. Phys.* **2014**, *141*, 164706.
- (S4) Jain, A.; Hautier, G.; Ong, S.; Moore, C.; Fischer, C.; Persson, K.; Ceder, G. Formation Enthalpies by Mixing GGA and GGA + U Calculations. *Phys. Rev. B* **2011**, *84*, 045115.
- (S5) Franchini, C.; Reticcioli, M.; Setvin, M.; Diebold, U. Polarons in Materials. *Nat. Rev. Mater.* **2021**, *6*, 560–586.
- (S6) Biškup, N.; Martínez, J. L.; Arroyo y de Dompablo, M. E.; Díaz-Carrasco, P.; Morales, J. Relation between the Magnetic Properties and the Crystal and Electronic Structures of Manganese Spinel LiNi_{0.5}Mn_{1.5}O₄ and LiCu_{0.5}Mn_{1.5}O_{4-δ} ($0 < \delta < 0.125$). *J. Appl. Phys.* **2006**, *100*, 093908.
- (S7) Streltsov, S. V.; Pchelkina, Z. V.; Khomskii, D. I.; Skorikov, N. A.; Anokhin, A. O.; Shvachko, Yu. N.; Korotin, M. A.; Anisimov, V. I.; Ustinov, V. V. Nature of the Ferromagnetic Ground State in the Mn₄ Molecular Magnet. *Phys. Rev. B* **2014**, *89*, 014427.
- (S8) Moorhead-Rosenberg, Z.; Chemelewski, K. R.; Goodenough, J. B.; Manthiram, A. Magnetic Measurements as a Viable Tool to Assess the Relative Degrees of Cation Ordering and Mn³⁺ Content in Doped LiMn_{1.5}Ni_{0.5}O₄ Spinel Cathodes. *J. Mater. Chem. A* **2013**, *1*, 10745–10752.